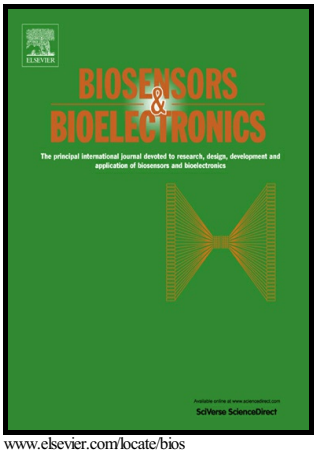

www.elsevier.com/locate/bios

Label-free ultrasensitive detection of breast cancer miRNA-21 biomarker employing electrochemical nano-genosensor based on sandwiched AgNPs in PANI and N-doped graphene

Razieh Salahandish, Ali Ghaffarinejad, Eskandar Omidinia, Hossein Zargartalebi, Keivan Majidzadeh-A, Seyed Morteza Naghib, Amir Sanati-Nezhad

PII: S0956-5663(18)30621-3
DOI: https://doi.org/10.1016/j.bios.2018.08.025
Reference: BIOS10689

To appear in: *Biosensors and Bioelectronic*

Received date: 29 May 2018
Revised date: 10 August 2018
Accepted date: 10 August 2018

Cite this article as: Razieh Salahandish, Ali Ghaffarinejad, Eskandar Omidinia, Hossein Zargartalebi, Keivan Majidzadeh-A, Seyed Morteza Naghib and Amir Sanati-Nezhad, Label-free ultrasensitive detection of breast cancer miRNA-21 biomarker employing electrochemical nano-genosensor based on sandwiched AgNPs in PANI and N-doped graphene, *Biosensors and Bioelectronic,* https://doi.org/10.1016/j.bios.2018.08.025

Label-free ultrasensitive detection of breast cancer miRNA-21 biomarker employing electrochemical nano-genosensor based on sandwiched AgNPs in PANI and N-doped graphene

Razieh Salahandish[a,b,c,d], Ali Ghaffarinejad[a,b*], Eskandar Omidinia[e*], Hossein Zargartalebi[c,d], Keivan Majidzadeh-A[f*], Seyed Morteza Naghib[g], Amir Sanati-Nezhad[c,d*]

[a]*Research Laboratory of Real Samples Analysis, Faculty of Chemistry, Iran University of Science and Technology (IUST), Tehran 1684613114, Iran*
[b]*Electroanalytical Chemistry Research Center, Iran University of Science and Technology (IUST), Tehran 1684613114, Iran*
[c]*BioMEMS and Bioinspired Microfluidic Laboratory, Department of Mechanical and Manufacturing Engineering, University of Calgary, Calgary T2N 1N4, Alberta, Canada*
[d]*Center for BioEngineering Research and Education, University of Calgary, Calgary T2N 1N4, Alberta, Canada*
[e]*Department of Biochemistry, Genetic and Metabolism Research Group, Pasteur Institute of Iran, Tehran, Iran*
[f]*Biomaterials and Tissue Engineering Department, Breast Cancer Research Center, Motamed Cancer Institute, ACECR , Tehran , Iran*
[g]*Nanobioengineering Division, Department of Nanothechnology, School of New Technologies, Iran University of Science and Technology (IUST), P.O. Box 16846-13114, Tehran, Iran*

ghaffarinejad@iust.ac.ir

eomid8@gmail.com

kmajidzadeh@razi.tums.ac.ir

amir.sanatinezhad@ucalgary.ca

[*]Corresponding authors.

Abstract

MicroRNAs (miRNAs) are small, endogenous, noncoding RNAs, shown to be expressed abnormally in many tumors and identified as predictive biomarkers for early diagnosis of several cancers including the breast. Therefore, the label-free and highly sensitive detection of miRNAs is of critical significance. In this work, a highly sensitive and label-free nano-genosensor is developed for the detection of miRNA-21, a known breast cancer biomarker, based on a specific

architecture of nitrogen-doped functionalized graphene (NFG), silver nanoparticles (AgNPs), and polyaniline (PANI) that resulted in a remarkable effect on signal amplification. Following the successful functionalization of the nanocomposite and immobilization of the specific sequence of the aminated complementary oligonucleotide of miRNA-21, the detection was performed using differential pulse voltammetry (DPV). The oxidation peak current of the redox probe under optimal conditions was determined to monitor the event hybridization of miRNA-21 biomarker. Applying this highly sensitive and optimized nano-biosensor enabled detection of a wide dynamic range of 10 fM - 10 µM with a sensitivity of 2.5 $\mu A.cm^{-2}$ and a low detection limit of 0.2 fM. This nano-biosensor also demonstrated highly reproducible results in the analysis of blood samples, with recoveries between 94 to 107%, and could be used for early detection of breast cancer by direct detection of the miRNA-21 in real clinical samples without any need to sample preparation, RNA extraction and/or amplification.

KEYWORDS: MiRNA-21; Electrochemical nano-genosensor; Nitrogen-doped modified graphene; Silver nanoparticle; Polyaniline; Breast cancer

1. Introduction

MiRNAs are sequences with an approximate length of 22 nucleotides that act as regulatory non-coding RNAs (Asaga et al. 2011). The role of miRNAs in controlling various physiological and pathological processes leads these molecules to be currently featured as biological markers in various diseases such as cancer, viral diseases cardiovascular disorders, and metabolic disorders (Acunzo et al. 2015). MiRNA-21 is particularly one of the most important miRNAs as a promising biomarker in diagnosis, prognostics, and therapy of breast cancer (Iorio et al. 2005; Sempere et al. 2007).

Various techniques have been developed for the detection of miRNAs, including Northern blot (Herbert et al. 2013), in situ hybridization (Deo et al. 2006), reverse transcription polymerase chain reaction (RT-PCR) (Markou et al. 2008), microarrays (Yan et al. 2008), and surface plasmon resonance (Zhou et al. 2011). The standard methods of Northern blot and in-situ hybridization are labor-intensive and have shown limited sensitivity, which make them cumbersome for routine clinical use (Válóczi et al. 2004; Yamamichi et al. 2009). The constraints of RT-PCR in detecting mature miRNAs expression and the potential distortion of gene expression have limited its selectivity (Markou et al. 2008). Other label-based techniques such as microarrays, surface plasmon resonance, and chemiluminescence that require fluorescent dyes to detect the hybridization of target miRNA, are expensive and time-consuming techniques and need commercial kits (Deng et al. 2013; Lodes et al. 2009; Wang et al. 2016). Therefore, electrochemical biosensors are elected as an appropriate technique due to their highly sensitive and selective performance, rapid, label-free, simple, and ease of automation in the detection of biomarkers in biofluids (Li et al. 2014; Zhang et al. 2015).

Several electrochemical biosensors with different surface functionalization protocols have been developed for the detection of miRNAs (Cai et al. 2013; Ge et al. 2014; Labib et al. 2013; Wen et al. 2012). Significant advances in the sensitivity (detection of miRNAs down to 5 fM resolution) by monitoring miRNAs hybridization have been relying on miRNAs labeled with nanoparticles or enzymes. However, these techniques still require to label or enrich miRNAs and therefore need several pre-processing operations (Gao and Yang 2006; Gao and Yu 2007). Further advances on label-free hybridization-based electrochemical sensors enabled rapid, selective, and sensitive detection of mature miRNAs and demonstrated that label-free electrochemical techniques can be a reliable alternative to the existing detection techniques

(Dong et al. 2013; Palecek and Bartosik 2012; Po□hlmann and Sprinzl 2010). However, the sensitivity, selectivity, and detection limit of miRNAs using direct electrochemical sensing is still a remaining challenge given the very low abundance and small size of these molecules in biofluids (Leshkowitz et al. 2013; Miao et al. 2015). Electrochemical nano-biosensors have combined the advantages of electrochemical biosensing with conductive nanocomposites and nanoparticles with enhanced surface area and catalytic properties to generate a new class of ultrasensitive diagnostics, reliable sensing, and easy-to-use assays (Hou et al. 2015; Li et al. 2016). Nano-biosensors have also been used for the direct and single step electrochemical detection of miRNAs (Daneshpour et al. 2016; Liu et al. 2015; Tian et al. 2018). We also recently demonstrated that optimizing combined nanoparticles and conductive nanocomposites can significantly enhance the sensing performance. Once optimized, these can be used for a highly sensitive detection of cancer proteins (Salahandish et al. 2018a-b). There is an immediate need for ordered architecture of the nanocoating to achieve more active binding sites on the electrode and provide a highly sensitive and selective electrochemical nano-biosensor for the detection of miRNAs.

In this study, a nanoscale label-free electrochemical biosensor with high sensitivity and selectivity is fabricated for the detection of miRNA-21 in a direct reading of blood samples. The nano-biosensor is based on silver nanoparticles (AgNPs) grafted on a functionalized graphene and nanostructured polyaniline (PANI) nanocomposite film. A functionalized three layers nanocomposite was deposited on the surface of the electrode step by step, followed by immobilizing the selective single stranded DNA (ss-DNA) as a complementary probe of miRNA-21. The assembly of layers was optimized considering critical variables. This nanocomposite architecture allowed more biomolecules to be immobilized at the electrode

surface, which reduced the distance for electron transfer and ion diffusion paths between the capture probe and nanomaterials. The nano-biosensor showed high determination sensitivity for miRNA with a very wide dynamic detection range of 10 fM - 10 μM and a low detection limit of 0.2 fM. Hence, the sensitive miRNA-21 nano-biosensor developed here may be well suited for the early detection of breast cancer.

2. Experimental

2.1. Chemicals and reagents

The graphite fine powder (spectroscopic grade, particle size ≤ 50 μm), sodium nitrate ($NaNO_3$), silver nitrate ($AgNO_3$), potassium nitrate (KNO_3), sulfuric acid (H_2SO_4, purity 98%), potassium permanganate ($KMnO_4$), potassium ferrocyanide $K_4Fe(CN)_6$, and potassium ferricyanide ($K_3Fe(CN)_6$) were purchased from Merck. 1-Ethyl-3-(3 dimethylaminopropyl) carbodiimide hydrochloride (EDC, purity 98%), N-hydroxysuccinimide (NHS, purity 98%), phosphate-buffered saline (PBS), dimethylformamide (DMF), 11-mercapto-1-undecanol (MU), and aniline (purity 99%) were purchased from Sigma-Aldrich. Fluorine doped tin oxide (FTO) electrodes were purchased from Solaronix. All miRNAs used in this work were purchased from BioNeer Company and dissolved in DNase/RNase-free distilled water and stored at -20 °C. Aqueous solutions were made with ultrapure deionized and enzyme-free water. A pH 7.4 PBS (20 mM PBS+0.15 M NaCl) was prepared as the supporting electrolyte for quantification using differential pulse voltammetry (DPV).

2.2. Methods and apparatus

Investigating the surface specifications of the nanocomposite components demands characterization tests. The quantity of Ag in the composition was measured by an Atomic

Absorption Spectrometer (AAS) equipped with a GFA-EX7 graphite furnace (Shimadzu AA 6300). The Field Emission Scanning Electron Microscopy (FESEM) images and mapping analysis were obtained by Carl Zeiss FESEM instrument model Sigma. The Atomic Force Microscopy (AFM) was performed by DPN5000 and using the silicon material noncontact tip. The Transmission Electron Microscopy (TEM) micrographs were obtained using the FEI Tecnai TF20 at 200 kV. All electrochemical studies were performed using an Autolab PGSTAT 30 (Echo chemie, B. V., Netherlands) Potentiostat/Galvanostat by Nova 1.11 software and employing the three-electrode system that contained an Ag/AgCl reference electrode, a platinum rod as the auxiliary electrode, and a modified FTO as the working electrode. The Electrochemical Impedance Spectroscopy (EIS) measurements were accomplished within the frequency range of 10^{-1}–10^{5} Hz, with the potential amplitude of 14 mV around the open circuit potential (E_{ocp}) in the $Fe(CN)_6^{3-/4-}$ and PBS buffer. All electrodes were tested three times for each experiment to establish error bars. Glassware was autoclaved and kept in an appropriate place to eliminate the effect of DNases and RNases on the stability of miRNAs.

2.3. Preparation of the nanocomposite-nanoparticle coated electrodes

The process of nano-biosensor preparation and functionalization that uses the sandwich NFG/AgNPs/PANI nanocomposite for the detection of miRNA-21 is schematically presented in **Fig. 1**. The fabrication procedure starts with polishing the bare FTO electrode (8 Ω resistance) and exposing it to sequential ultrasonic cleaning in acetone, ethanol, isopropanol, and deionized (DI) water for 10 min and dried under an argon flow. The graphene oxide was synthesized by modified Hummer using graphite fine powder, $NaNO_3$, H_2SO_4, and $KMnO_4$ according to the literature (Li et al. 2013). The graphene oxide was functionalized using 400 μM EDC and 100

μM NHS prepared in DI water. The functionalized product was reduced using DMF and washed with DI water to produce N-doped functionalized graphene (NFG), in which the carbon monoxide released from DMF in its boiling point (Cernat et al. 2015; Li et al. 2013). The NFG suspended in DI water (2.5 $mg.mL^{-1}$) was then deposited on the FTO surface by cast coating, in which the optimal volume was found to be 40 μL following 60 min of drying (Salahandish et al. 2018a-a). The electrodeposition of the middle AgNP layer over the NFG was implemented in 1 mM $AgNO_3$/0.1 M KNO_3 electrolyte using dual potential chronoamperometry technique (E_1 and t_1; -0.4 V, 1 and 10 s; E_2 and t_2; 0.34 V, 30 and 90 s, respectively) (Ustarroz et al. 2010). Briefly, the PANI layer was electropolymerized on the electrode surface utilizing a mixture of 0.5 M H_2SO_4 and 0.03 M aniline in which the adjusted parameters for this purpose were scan rate of 30 $mV.s^{-1}$ for 20 scan cycles within the potential range of -0.4 to 1.2 V (Darowicki and Kawula 2004). Microscopic techniques of AFM, FESEM, and TEM were used to ensure specification and quality of the coated electrode and synthesized nanocomposite. The protocols for the synthesis and optimization of the nanocomposite structure is explained in detail elsewhere (Salahandish et al. 2018a-b).

2.4. Probe immobilization

To bind bioreceptors on top of the modified electrode, the NFG/AgNPs/PANI nanocomposite fabricated on the FTO electrode surface was functionalized by carboxyl functional group in NHS/EDS solution for 4 hrs. Subsequently, aminated complementary ss-DNA of miRNA-21 as a probe with the sequence of 5′-NH-TCAACATCAGTCTGATAAGCTA-3′ was immobilized on the surface of working electrode through amidic bonding overnight at room temperature (Chen et al. 2008; Li et al. 2013; Wang and Vo- Dinh 2011; Zhou et al. 2010). The functionalized

electrodes were incubated with 1 mM MU for 30 min at room temperature to orient the complementary probes and block the unoccupied spaces among them.

2.5. Sensing performance and optimization

A label-free sensing process was adopted at 37 °C under 80% humidity for 30 min. Different standard concentrations of target miRNA solution in the hybridization buffer were employed to develop calibration curves against a plethora of miRNA-21 concentrations over the target sequence of 5′-UAGCUUAUCAGACUGAUGUUGA-3 (Song et al. 2010; Wang et al. 2014b; Wei et al. 2011; Zhang et al. 2011) and determine the dynamic range of detection. The electrodes were rinsed with PBS to eliminate non-specific miRNA bindings. Finally, a PBS solution (0.02 M, pH = 7.4) containing 2.5 mM $K_3Fe(CN)_6$ and 2.5 mM $K_4Fe(CN)_6$ was used as a redox probe, and the current signals, utilizing DPV, were recorded. Different parameters affecting the sensing efficiency, including the probe concentration, reaction time, temperature, and pH were optimized to achieve the highest sensitivity. For the control, the nano-biosensor was immersed in MU solution without hybridization with target miRNA. The selectivity of the sensor was also evaluated using a non-complimentary miRNA with the sequence of 5′-GUAAGGCAUCUGACCGAAGGCA-3′.

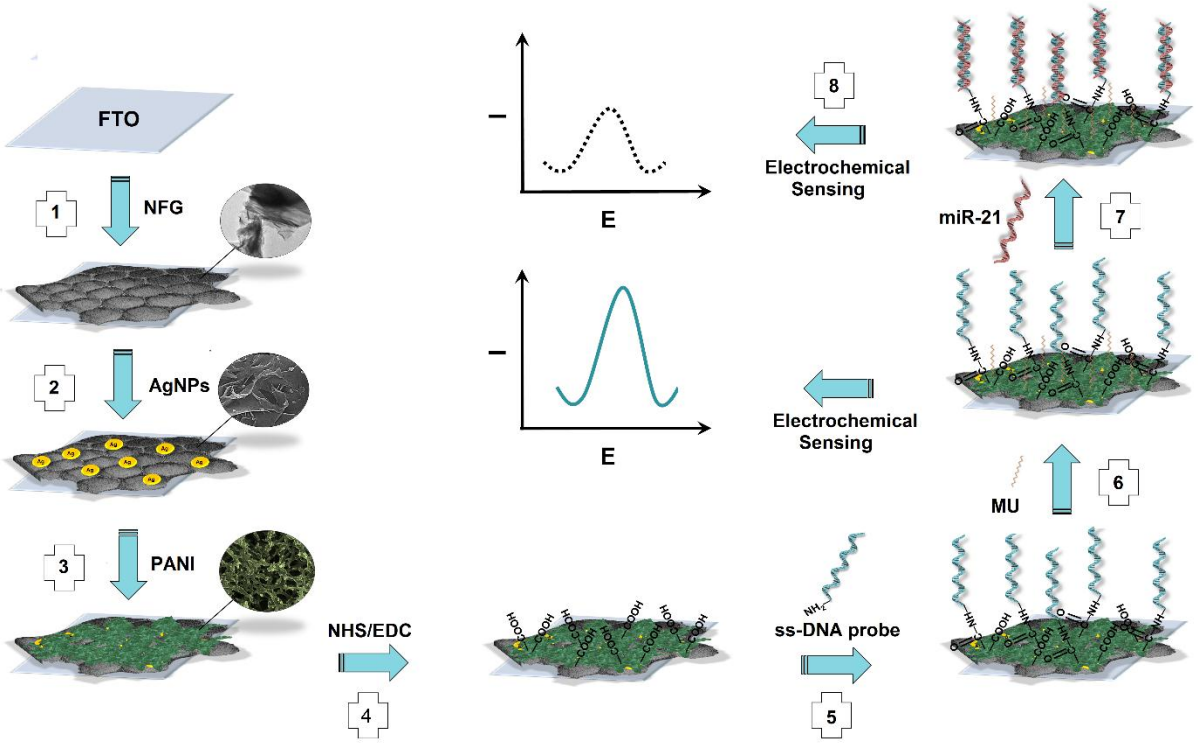

Fig. 1. The schematic of various steps of nanocomposite fabrication; 1) Depositing N-doped functionalized graphene (NFG) over a surface of fluorine doped tin oxide (FTO) electrode; 2) Electrodeposition of silver nanoparticles (AgNPs); 3) Electropolymerization of polyaniline (PANI) over the NFG/Ag substrate; 4) Functionalization of the surface with carboxylic functional group using N-hydroxysuccinimide (NHS)/1-Ethyl-3-(3 dimethylaminopropyl) carbodiimide hydrochloride (EDC); 5) Adsorption of single stranded DNA (ss-DNA) probe using modified electrode by NHS/EDC; 6) Adding 11-mercapto-1-undecanol (MU) for blocking all the blanked areas and orienting the bonded miRNA-21 complementary probes; 7) Biological capturing miRNA-21 target through bioreceptors; 8) Evaluation of electrochemical sensing process employing differential pulse voltammetry (DPV) and comparing the signals for different steps of the electrode functionalization and hybridization (sensing).

3. Results and Discussions

3.1. Characterization of NFG/AgNPs/PANI nanocomposite

The NFG layer was coated on the surface of the electrode substrate in pursuance of rising the surface area and conductance of the charge transfer. The thickness and surface roughness of the deposited materials as well as the number of layers of graphene nanosheets were characterized

by AFM analysis. Two and three-dimensional images of dried NFG (dispersed in DMF solvent) on the fresh mica substrate are shown in **Fig. S1**. The AFM scan of the surface of three graphene sheets and one graphene sheet with higher magnification are shown in **Fig. S1A** and **B**, respectively. Cross-sectional analysis was used to analyze the details of AFM images. The dispersion of graphene nanosheets with different heights is shown in **Fig. S1C**, demonstrating that the highest dispersion was detected for the graphene with a thickness of about 10 nm while there exists a few layers of graphene with a thickness about 2 nm. It is also worth mentioning that the round shape of the white dots are relates to the folded structure of the graphene sheets.

Different nanoparticles such as Ag, gold (Au), and copper (Cu) have been examined as the interface layer between the upper PANI layer and the bottom NFG substrate to intensify the nanocomposite charge transfer conductivity and increase the bonding strength between the layers. It was found that CuNPs prevent PANI formation due to formation of the oxidation-prone electrodeposited nanoparticles in the applied potential for PANI electropolymerization (**Fig. S2**). Furthermore, comparing the cyclic voltammograms of nanocomposites NFG/AgNPs/PANI and NFG/AuNPs/PANI showed that, having more kinetic, charge transfer conductivity, and stability, the Ag nanoparticles, as a sandwiched layer, were more appropriate for sensing with respect to Au (**Fig. S3**). The FESEM images of different AgNPs sizes are shown for different deposition parameters of dual potential chronoamperometry in which the duration E_1 was dedicated to the deposition of AgNPs cores and the duration E_2 was devoted to the growth of cores (**Fig. 2A-D**). The more the electrodeposition duration, the more the deposition of cores and the larger the size of NPs. AAS was performed to obtain the concentration of AgNPs on the NFG electrode surface (**Table S1**). Moreover, to rationalize the amount of Ag with the coulombic charge (Q) passed through the electrode, the area under dual potential chronoamperometry curve regarding the

deposition of Ag was calculated for various durations. The results show that the surface concentration of the deposited Ag is an increasing function of *Q* (**Fig. S4**).

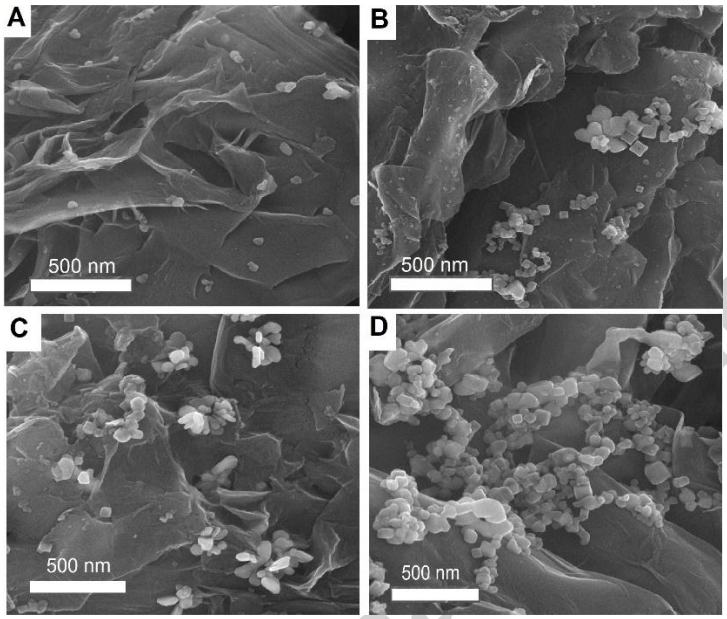

Fig. 2. The field emission scanning electron microscopy (FESEM) images of NFG/Ag with the deposition duration of **(A)** 1 s and 30 s, **(B)** 1 s and 90 s, **(C)** 1 s and 150 s, and **(D)** 10 s and 90 s for E_1 and E_2, respectively, for synthesizing AgNPs using dual potential chronoamperometry technique.

The PANI layer was finally electropolymerized as the last (top) layer which further increased the conductivity and effective surface area of the electrode in order to enhance the sensitivity of the sensor and improve the interaction with miRNA-21 complementary probe (Wang et al. 2014a). The micrographs of nanocomposite in different steps are depicted in **Fig. 3**. The underlying transparent NFG sheets at the bottom layer increase the adhesion properties for the subsequent layers (**Fig. 3A**). The decorated AgNPs on NFG surface (**Fig. 3B**) increase the surface area for bonding the capture molecules to the surface while the pellet/flake-like structure of PANI provides a proper substratum for better attachment of miRNA-21 complementary probe to the nanocomposite coating (**Fig. 3C**).

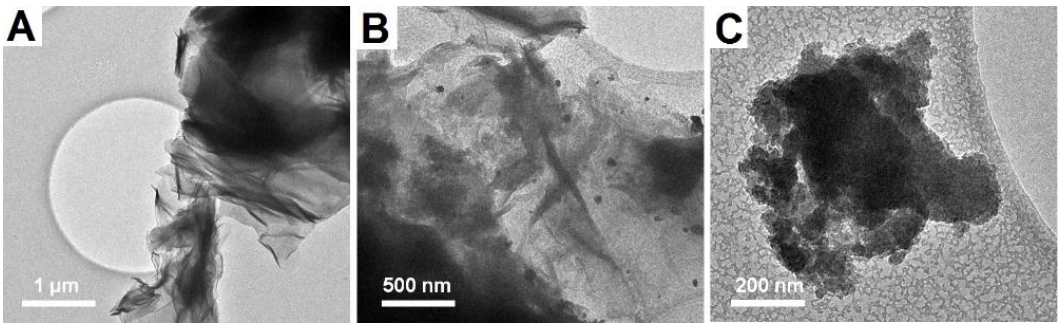

Fig. 3. Transmission Electron Microscopy (TEM) micrographs of **(A)** few-layer NFG, **(B)** NFG decorated by Ag, and **(C)** pellet/flake-like structure of NFG/Ag/PANI.

3.2. Electrochemical characterizing the modified electrode surface

The Nyquist and Bode modulus plots are impedance spectra used as criteria to electrochemically evaluate the surface characterizations during the nanocomposite-based modification process (in each step of modification), MU, miRNA-21 complementary probe, and miRNA-21 target in $Fe(CN)_6^{3-/4-}$ redox probe (**Fig. S5** and **Fig. 4**). The diameters of semicircles in **Fig. S5** and **Fig. 4A** are an indication of charge transfer resistance (R_{ct}) which for the bare FTO is approximately 11,000 Ω. Step by step modification of the electrode surface induces considerable decrease in R_{ct}. This implies that all the applied components in the sandwich-like nano-structure have synergic effects that reduce the resistance noticeably, meaning a huge enhancement in sensitivity and decline in detection limit (**Fig. 4A, a**). Next, the oligonucleotide sequence probe is attached to NFG/AgNPs/PANI via amid covalent bond formation between the carboxylic group on the nanocomposite and amino group of the ss-DNA probe. Adding the oligonucleotide probe on the surface drastically increases R_{ct} due to steric hindrance, making the access of redox probe to the electrode for charge transfer difficult. Moreover, this probe causes charge repulsion between oligonucleotide (because of negative charge of phosphate) and redox probe of $Fe(CN)_6^{3-/4-}$ which leads to R_{ct} augmentation (**Fig. 4A, b**). Therefore, since the ss-DNA probe, MU, and miRNA are

non-electroactive molecules, their immobilization on the electrodes serves as a blocking layer, reducing the effective area over the electrode and accordingly preventing electron transfer to the functionalized electrode (**Fig. 4A, b-d**). Bode modulus can be used to indicate the resistance changes with respect to frequency (ω). Comparing the **Fig. 4A** and **4B**, both showed that there is a precise correspondence between Nyquist and Bode plots. Considering the Bode modulus, when ω tends to 0 and □, the value of $|Z|$ tends to $R_s + R_{ct}$ and R_s, respectively, in which R_s denotes solution resistance. Consequently, $|Z|$ appears as a strictly descending function of ω (**Fig. 4B**). To further study the EIS plot, the equivalent circuits were extracted for each step of the electrode functionalization and detection process (**Table S2**). All these steps excluding the hybridization step were fitted by [R([RW]Q)] equivalent circuit. W is Warburg diffusion element and is related to mass-transfer controlled zone with a linear behavior in low frequencies. Q is a constant phase element (CPE) and observed when there is no ideal double-layer electrical capacitor (C_{dl}) behavior due to the roughness and porosity of the electrode surface as well as the lack of complete surface uniformity. However, there is no Warburg element in the hybridization step given the fact that the behavior of the electrode is completely under control of kinetics at low frequencies. Moreover, applying the potential leads to charge accumulation on the electrode surface and consequently moving the ions and polar molecules with the opposite charge towards the electrode and creating an electrochemical capacitor. This charge accumulation would not occur when the surface is blocked by non-conductive modifier materials under the applied potential, representing the decrease in the capacitance.

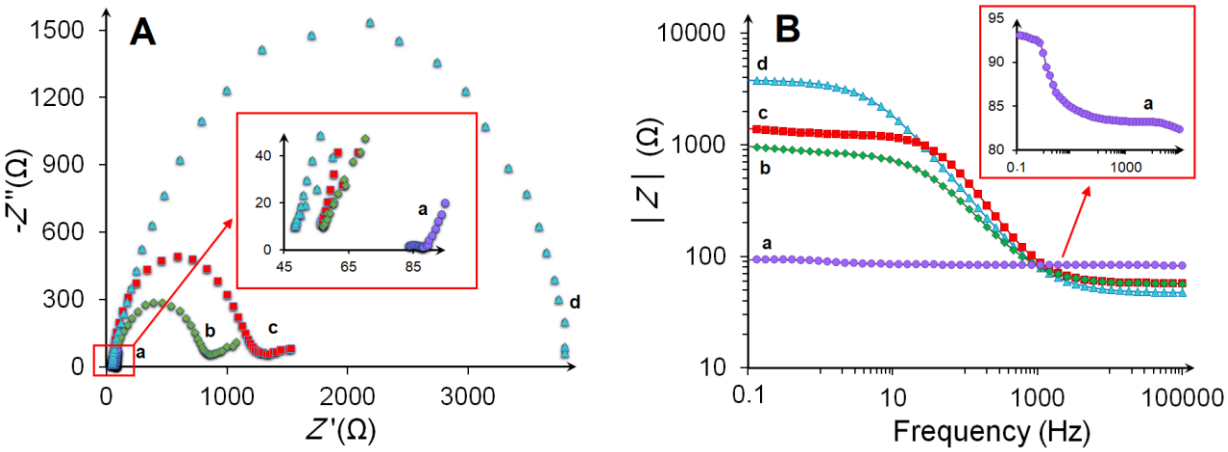

Fig. 4. Electrochemical Impedance Spectroscopy (EIS) data including **(A)** Nyquist and **(B)** Bode modulus plots for different modification steps; **a)** the NFG/AgNPs/PANI nanocomposite, **b)** nanocomposite/ss-DNA probe, **c)** nanocomposite/ss-DNA probe /MU, and **d)** nanocomposite/ss-DNA probe /MU/target miRNA in a solution containing 2.5 mM $K_3Fe(CN)_6$ + 2.5 mM $K_4Fe(CN)_6$ and 0.02 M PBS.

The DPV technique is adopted for sensing evaluations. This method relies on label-free electrochemical signal of $Fe(CN)_6^{3-/4-}$ as a redox probe. The DPV method was used to measure the difference between current density of the blank state (which is related to the deposited MU on top of the electrode) and the certain concentration of the hybridized target with the ss-DNA probe, namely Δj. The presence of non-electroactive microRNAs on the surface of the electrode affects the magnitude of current peak. In other words, the peak amplitude is used to detect the concentrations of miRNA. Also the quantitative evaluation of different steps of electrode modification confirms that the bare FTO electrode results in a negative Δj, while the incorporation of subsequent layers of nanocomposite increases the Δj value staying in the positive range (**Fig. S6**).

3.3. Optimization of sensing conditions

Several crucial sensing parameters, including ss-DNA probe concentration, interaction time, temperature, and pH that play central role in the sensing performance demand optimization. To evaluate the repeatability of the nano-genosensor, all tests were repeated three times each. The concentration of the probe was further optimized for different probe concentrations of 1×10^{-10}, 2×10^{-10}, 5×10^{-10}, 1×10^{-9}, 2×10^{-9} and 1×10^{-8} M (**Fig. S7A**). It is shown that at low probe concentration (less than 1×10^{-9} M), Δj is an increasing function of the ss-DNA probe concentration. Increasing the probe concentration leads to a better interaction between the probe and miRNA-21 which culminates in Δj augmentation. Since miRNA is a non-electroactive biomaterial, following the probe and miRNA hybridization, the peak of current density (j) decreases and the difference between the current density for the hybridization and bare state increases. However, for concentrations over 1×10^{-9} M, Δj becomes independent from the probe concentration. From a certain value of the probe concentration, the surface of the electrode becomes saturated, and applying more probes to the solution does not influence Δj (Xu et al. 2001). The interaction time between the miRNA-21 and the ss-DNA probe is another significant parameter that needs to be optimized. Accordingly, to optimize this parameter, various hybridization times, including 15, 30, 60, 120, and 180 min were experimented. The results show that the optimal interaction time is about 30 min where all required hybridizations are performed in this period (**Fig. S7B**).

Temperature of electrolyte has also noticeable effect on the electrochemical response. Hence, the performance of the nano-biosensor was evaluated at different temperatures (26, 35, 45, 55, and 65 °C). Given the fact that biomolecules are naturally highly sensitive to heat, the optimum working temperature of $Fe(CN)_6^{3-/4-}$ solution for detecting the biomolecules was determined to be 35 °C which is near the human physiological temperature. Increasing the

temperature above 35 °C denatures the miRNAs and oligonucleotide probes (**Fig. S7C**) (Zhu et al. 2012). Finally, pH is the last parameter to be optimized. A highly acidic incubation medium may lead to the decomposition of nucleic acids to their components, i.e. sugar, bases, phosphate and a weak acidic state may cause the disruption of miRNA sequence. Moreover, hydrogen bonds between the pair of primes may divide the miRNA structure. To assess the effect of pH on the stability of the biosensors, the sensing was performed for different electrolytes with various pH values. It is shown that the optimal pH value of 7.4 provides a highly efficacious biosensing (**Fig. S7D**). It is worth mentioning that the calculated repeatability and reproducibility were RSD ≤ 7 and ≤ 3, respectively. Following the optimization of the functionalization parameters, the optimal values are adopted for the biosensing experiments, including sensor calibration and real-sample testing.

3.4. Sensitivity, selectivity, and reproducibility of miRNA-21 nano-biosensor

Following optimization of the coating and incubation procedure, all the analytical experiments were performed under the optimal conditions. The nano-biosensor demonstrated a great sensitivity in detection of various miRNA-21 concentrations within 30 min incubation time. DPV is one of the most potent and commonplace electroanalytical methods utilized for electrochemical measurements and characterizing surface interfaces. In this work, the DPV technique was adopted to assess the change of electrochemical response after MU treatment and hybridization of the capture probe with miRNA target (**Fig. 5A**). The current density peak after hybridization with the target miRNA, at a concentration of 1×10^{-14}, was about four times smaller than before hybridization event and about eight times smaller after immobilization of the capture probe over the electrode. The distinction between the current densities of hybridization step and MU-treated electrode (Δj) is sufficiently high to quantify target miRNA with high resolution. At

least, three replicates were examined for each miRNA-21 concentration to obtain the calibration curve (**Fig. 5B**). The calibration curve depicts ultrasensitive response with the ability of detecting low concentration of the miRNA-21. The Δj is shown to be linearly correlated against the logarithmic of miRNA concentration attaining a wide linear range of 10 fM to 10 μM with the sensitivity of 2.5 $\mu A.cm^{-2}$ and $R^2 = 0.9953$. Moreover, the detection limit of 0.2 fM (S/N=3) and quantification limit of 9.4 fM (S/N=10) were obtained. All RSDs are less than 8% showing that several nano-biosensors can be prepared simultaneously for detection assays. The performance of our biosensor was compared to the existing sensors in the literature used for the detection of miRNA-21 (**Table S3**).

To evaluate the matrix effect, the selectivity of the nano-biosensor was investigated by a comparison study between the mismatch and miRNA-21 targets with the same concentration (1 μM) and for 30 min of incubation, as used in the calibration process, in the DNase/RNase free distilled water and blood. As expected, the current signal difference of miRNA-21 target is much higher than the electrochemical signal of non-complementary sequence in both media, indicating high selectivity of the nano-biosensor over interferences (**Fig. 5C**). In addition, the blood sample including both miRNA-21 and mismatch targets was tested to evaluate the effect of other non-complementary miRNAs in the efficiency of the nano-genosensor. The results show that there is no significant difference between the result of the blood sample containing both miRNA-21 and mismatch targets and the blood sample comprising only miRNA-21.

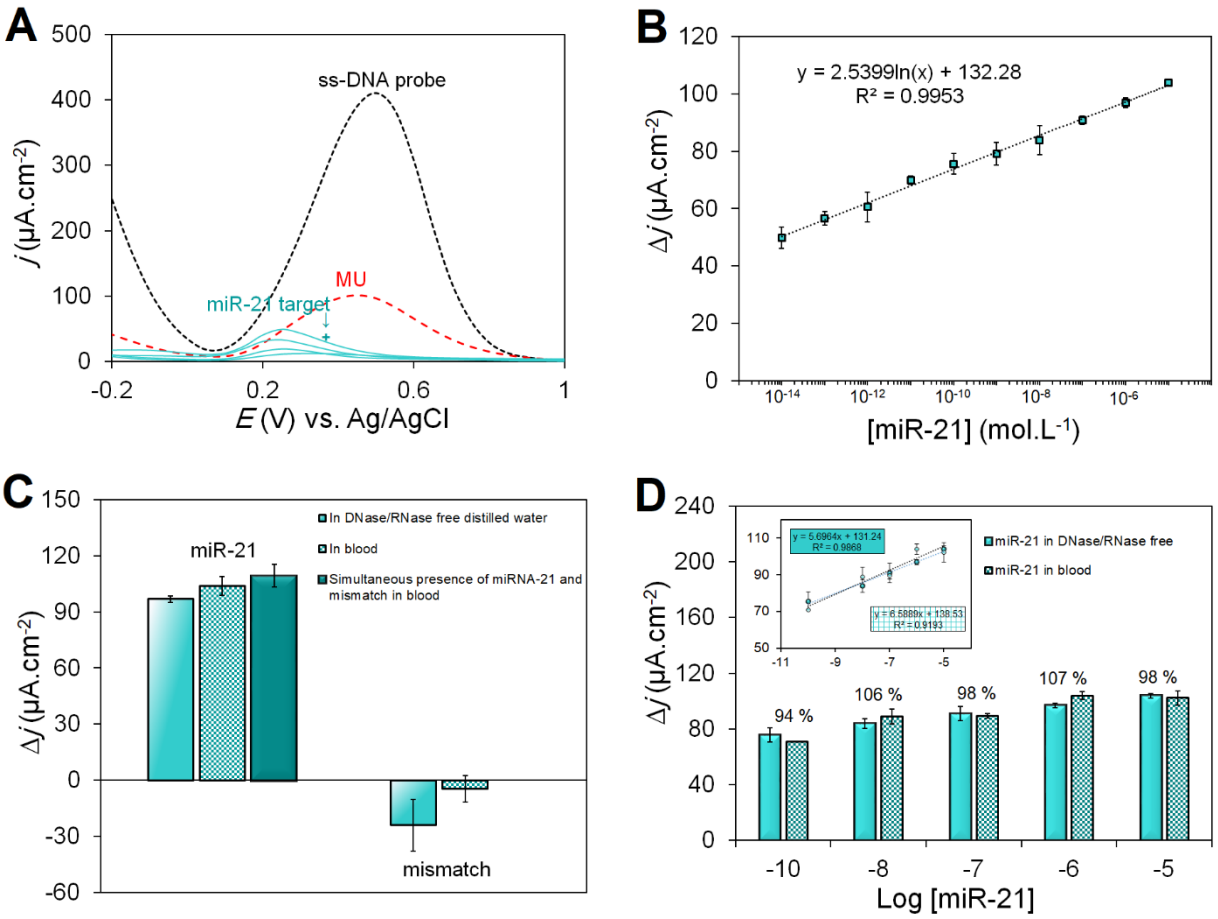

Fig. 5. Different tests for investigating the nano-genosensor performance. **(A)** DPV plot showing noticeable changes among three steps of ss-DNA probe immobilization, MU treatment, and miRNA-21 target capture on the electrode; **(B)** The calibration curve shows a linear range of detection within the range of 10 fM – 10 μM with the sensitivity of 2.5 μA.cm^{-2} **(C)** The selectivity analysis comparing the detection of 1 μM miRNA-21 with the same concentration of mismatch target in the DNase/RNase free distilled water and blood; **(D)** Testing the nano-biosensor for comparing the detection of miRNA-21 in the blood and DNase/RNase free distilled water, demonstrating the high recovery of nano-biosensor for miRNA detection.

3.5. miRNA-21 assay in human blood samples

The primary objective of developing biosensors is to use them for the early and precise cancer detection. In this work, the DPV signals for the detection of three different miRNA-21 concentrations in the DNase/RNase free distilled water and blood were quantified in three

replications, with high recovery rates and low RSD percentages (**Fig. 5D**). In this respect, we spiked predefined concentrations of miRNA-21 into the blood samples as a complex matrix without any pretreatment. The results show the appropriate recoveries of 94%, 106%, 98%, 107%, and 98% for different concentrations of 1×10^{-10}, 1×10^{-8}, 1×10^{-7}, 1×10^{-6}, and 1×10^{-5} M, respectively (**Table 1**), demonstrating that the nano-biosensor is competent enough to detect miRNA-21 in real circumstances. The high recovery rate and low RSD percentage demonstrates the great functionality of the proposed nano-biosensor for the detection of target miRNA-21 in real blood samples without any need for cell separation, sample preparation, extraction, and amplification. Overall, no significant interference was observed in the sensors selectivity neither in the simple matrix, nor complex real blood.

Table 1. The recovery of miRNA-21 spiked in the blood and captured on the nano-biosensor.

Sample Number	Added log [miR-21]	Detected log [miR-21]	Recovery (%)	RSD (%) (n=3)
1	-10.0	-10.5	93.9	5.3
2	-8.0	-7.4	106.1	1.7
3	-7.0	-7.5	98	2.9
4	-6.0	-4.9	107.3	5.1
5	-5.0	-5.6	98	8.5

Conclusion

A favorable electrochemical nano-genosensor with the NFG/AgNPs/PANI electrode configuration was demonstrated as a high-performance sensing platform for rapid, quantitative

and highly sensitive and selective detection of miRNA-21 cancer biomarker. Employing cost effective materials, such as the FTO substrate and surface modifier nanocomposite for fabricating sensitive and stable sensing protocols, keeps this biosensor competitive in the marketplace. Moreover, the stable performance of the sensor upon being subjected to matrix effects and the ability for detecting the target miRNA-21 biomarker within the whole blood demonstrate its potential for clinical use without any need to preemptively process blood samples. This sensor, however, needs further clinical validation, miniaturization and sensing automation, directing it toward an autonomous point-of-care detection device. This rapid, robust, and affordable nano-genosensor offers significant reproducibility and repeatability, and also opens up an avenue for continual monitoring of changes in biomarker activity during medical treatment.

Acknowledgement

We gratefully acknowledge the support of this project by the Biotechnology Support Fund of Biotechnology Development Council; vice Presidency for Science and technology under grant No. 96/11204; excellent cooperation of Research Councils of Iran University of Science and Technology (IUST) (160.17636); the Natural Sciences and Engineering Research Council of Canada (NSERC) (10010499), and Canada Research Chair; Breast Cancer Research Center (BCRC) (IR.ACECR.IBCRC.REC.1395.9).

Notes

The authors declare no competing financial interests.

References

Acunzo, M., Romano, G., Wernicke, D., Croce, C.M., 2015. Advances in Biological Regulation 57, 1-9.

Asaga, S., Kuo, C., Nguyen, T., Terpenning, M., Giuliano, A.E., Hoon, D.S., 2011. Clinical Chemistry 57(1), 84-91.

Cai, Z., Song, Y., Wu, Y., Zhu, Z., Yang, C.J., Chen, X., 2013. Biosensors and Bioelectronics 41, 783-788

Cernat, A., Tertiş , M., Păpară, C.N., Bodoki, E., Săndulescu, R., 2015. Int. J. Electrochem. Sci 10, 4718-4731.

Chen, Y., Liu, W., Chao, T., Zhang, Y., Yan, X., Gong, Y., Qiang, B., Yuan, J., Sun, M., Peng, X., 2008. Cancer Letters 272(2), 197-205.

Daneshpour, M., Omidfar, K., Ghanbarian, H., 2016. Beilstein journal of nanotechnology 7, 2023.

Darowicki, K., Kawula, J., 2004. Electrochimica Acta 49(27), 4829-4839.

Deng, H., Ren, Y., Shen, W., Gao, Z., 2013. Chemical Communications 49(82), 9401-9403.

Deo, M., Yu, J.Y., Chung, K.H., Tippens, M., Turner, D.L., 2006. Developmental Dynamics 235(9), 2538-2548.

Dong, H., Lei, J., Ding, L., Wen, Y., Ju, H., Zhang, X., 2013. Chemical Reviews 113(8), 6207-6233.

Gao, Z., Yang, Z., 2006. Analytical Chemistry 78(5), 1470-1477.

Gao, Z., Yu, Y.H., 2007. Biosensors and Bioelectronics 22(6), 933-940.

Ge, Z., Lin, M., Wang, P., Pei, H., Yan, J., Shi, J., Huang, Q., He, D., Fan, C., Zuo, X., 2014. Analytical Chemistry 86(4), 2124-2130.

Herbert, K.M., Pimienta, G., DeGregorio, S.J., Alexandrov, A., Steitz, J.A., 2013. Cell Reports 5(4), 1070-1081.

Hou, T., Li, W., Liu, X., Li, F., 2015. Analytical Chemistry 87(22), 11368-11374.

Iorio, M.V., Ferracin, M., Liu, C.-G., Veronese, A., Spizzo, R., Sabbioni, S., Magri, E., Pedriali, M., Fabbri, M., Campiglio, M., 2005. Cancer Research 65(16), 7065-7070.

Labib, M., Khan, N., Ghobadloo, S.M., Cheng, J., Pezacki, J.P., Berezovski, M.V., 2013. Journal of the American Chemical Society 135(8), 3027-3038.

Leshkowitz, D., Horn-Saban, S., Parmet, Y., Feldmesser, E., 2013. RN 19(4), 527-538.

Li, F., Peng, J., Wang, J., Tang, H., Tan, L., Xie, Q., Yao, S., 2014. Biosensors and Bioelectronics 54, 158-164.

Li, H., He, J., Li, S., Turner, A.P., 2013. Biosensors and Bioelectronics 43, 25-29.

Li, W., Hou, T., Wu, M., Li, F., 2016. Talanta 148, 116-121.

Liu, L., Song, C., Zhang, Z., Yang, J., Zhou, L., Zhang, X., Xie, G., 2015. Biosensors and Bioelectronics 70, 351-357.

Lodes, M.J., Caraballo, M., Suciu, D., Munro, S., Kumar, A., Anderson, B., 2009. PloSOne 4(7), e6229.

Markou, A., Tsaroucha, E.G., Kaklamanis, L., Fotinou, M., Georgoulias, V., Lianidou, E.S., 2008. Clinical Chemistry 54(10), 1696-1704.

Miao, P., Wang, B., Yu, Z., Zhao, J., Tang, Y., 2015. Biosensors and Bioelectronics 63, 365-370.

Palecek, E., Bartosik, M., 2012. Chemical Reviews 112(6), 3427-3481.

Po□hlmann, C., Sprinzl, M., 2010. Analytical hemistry 82(11), 4434-4440.

Salahandish, R., Ghaffarinejad, A., Naghib, S.M., Majidzadeh-A, K., Sanati-Nezhad, A., 2018a-a. IEEE Sensors Journal 18(6), 2513 - 2519.
Salahandish, R., Ghaffarinejad, A., Naghib, S.M., Majidzadeh-A, K., Zargartalebi, H., Sanati-Nezhad, A., 2018a-b. Biosensors and Bioelectronics 117, 104-111.
Sempere, L.F., Christensen, M., Silahtaroglu, A., Bak, M., Heath, C.V., Schwartz, G., Wells, W., Kauppinen, S., Cole, C.N., 2007. Cancer Research 67(24), 11612-11620.
Song, B., Wang, C., Liu, J., Wang, X., Lv, L., Wei, L., Xie, L., Zheng, Y., Song, X., 2010. Journal of Experimental & Clinical Cancer Research 29(1), 29.
Tian, L., Qian, K., Qi, J., Liu, Q., Yao, C., Song, W., Wang, Y., 2018. Biosensors and Bioelectronics 99, 564-570.
Ustarroz, J., Gupta, U., Hubin, A., Bals, S., Terryn, H., 2010. Electrochemistry Communications 12(12), 1706-1709.
Válóczi, A., Hornyik, C., Varga, N., Burgyán, J., Kauppinen, S., Havelda, Z., 2004. Nucleic Acids Research 32(22), e175-e175.
Wang, H.N., Vo- Dinh, T., 2011. Small 7(21), 3067-3074.
Wang, L., Hua, E., Liang, M., Ma, C., Liu, Z., Sheng, S., Liu, M., Xie, G., Feng, W., 2014a. Biosensors and Bioelectronics 51, 201-207.
Wang, M., Fu, Z., Li, B., Zhou, Y., Yin, H., Ai, S., 2014b. Analytical Chemistry 86(12), 5606-5610.
Wang, Q., Liu, R., Yang, X., Wang, K., Zhu, J., He, L., Li, Q., 2016. Sensors and Actuators B: Chemical 223, 613-620.
Wei, J., Gao, W., Zhu, C.J., Liu, Y.Q., Mei, Z., Cheng, T., Shu, Y.Q., 2011. Chinese Journal of Cancer 30(6), 407-414.
Wen, Y., Pei, H., Shen, Y., Xi, J., Lin, M., Lu, N., Shen, X., Li, J., Fan, C., 2012. Scientific Reports 2, 867.
Xu, C., Cai, H., He, P., Fang, Y., 2001. Analyst 126(1), 62-65.
Yamamichi, N., Shimomura, R., Inada, K., Sakurai, K., Haraguchi, T., Ozaki, Y., Fujita, S., Mizutani, T., Furukawa, C., Fujishiro, M., 2009. Clinical cancer research 15(12), 4009-4016.
Yan, L.X., Huang, XF., Shao, Q., Huang, M.-Y., Deng, L., Wu, Q.L., Zeng, Y.X., Shao, J.Y., 2008. Rna 14(11), 2348-2360.
Zhang, A., Liu, Y., Shen, Y., Xu, Y., Li, X., 2011. Urology 78(2), 474. e413-474. e419.
Zhang, Y., Yan, Y., Chen, W., Cheng, W., Li, S., Ding, X., Li, D., Wang, H., Ju, H., Ding, S., 2015. Biosensors and Bioelectronics 68, 343-349.
Zhou, W.-J., Chen, Y., Corn, R.M., 2011. Analytical Chemistry 83(10), 3897-3902.
Zhou, X., Ren, Y., Moore, L., Mei, M., You, Y., Xu, P., Wang, B., Wang, G., Jia, Z., Pu, P., 2010. Laboratory Investigation 90(2), 144.
Zhu, Y., Chandra, P., Shim, Y.-B., 2012. Analytical Chemistry 85(2), 1058-1064.

Highlights

- **Ultrasensitive nano-genosensor for detection of miRNA-21 as a promising breast cancer biomarker**
- **A label-free repeatable and reproducible nano-biosensor with a very wide linear range**
- **High recovery regarding to electrochemically sense miRNA-21 in blood as a real sample without any pretreatment**